CHEMISTRY OF MATERIALS

pubs.acs.org/cm

Article

N-Heterocyclic Linkages Are Produced from Condensation of Amidines onto Graphitic Carbon

Seokjoon Oh, Ryan P. Bisbey, Sheraz Gul, Junko Yano, Gregory L. Fisher,* and Yogesh Surendranath*

Cite This: *Chem. Mater.* 2020, 32, 8512−8521

Read Online

ACCESS | Metrics & More | Article Recommendations | Supporting Information

ABSTRACT: Covalent chemical modification is a powerful strategy for endowing low-cost graphitic carbon substrates with designer functionality. However, the surface chemistry of carbon is complex, making it difficult to tailor carbon materials with molecular level precision. Herein, we establish a new chemical modification strategy that generates strong aromatic linkages to carbon surfaces. In particular, we show that the condensation of amidine-containing molecules with oxidic edge defects on carbon surfaces generates well-defined pyrimidine and imidazole linkages. X-ray photoelectron and nitrogen K-edge X-ray absorption near-edge structure spectroscopies along with time-of-flight secondary ion mass spectrometry tandem mass spectrometry analysis establish the molecular structures of the surface linkages. We find that the ring structure and nucleophilicity of the precursor molecule guide the selectivity of the surface condensation reaction, with 5−5 ring strain driving selective condensation to form pyrimidine linkages on zigzag edges. This work establishes new methods for functionalizing and analyzing carbon surfaces at the molecular level.

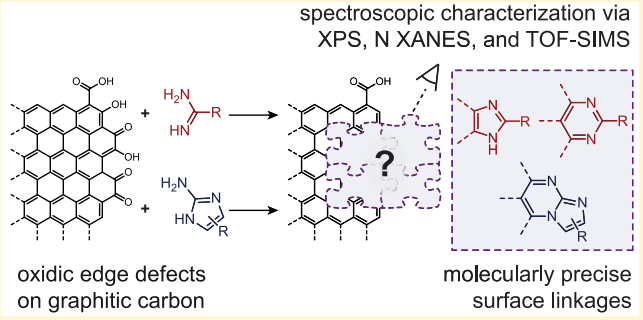

INTRODUCTION

Chemical modification of carbon surfaces transforms an inexpensive, ubiquitous conductor into a versatile functional material. Carbons are modified for use as catalyst supports, most notably for hydrogenation,[1,2] and for use as electrodes in sensors,[3] batteries,[4] solar cells,[5] supercapacitors,[6] electrolyzers,[7] and fuel cells.[8] In addition, there is growing interest in utilizing carbon as a host for grafting molecular active sites tailored for a wide variety of electrochemical and thermal catalytic applications.[9−12] For such catalytic applications, the linkage chemistry used to graft the catalytic active site onto carbon has a profound impact on efficiency and device performance.[13]

To gain predictive, molecular-level insights into the behavior of carbon-supported catalysts, linkage chemistries are desired that simultaneously satisfy several criteria. First, the local bonding arrangement in the linkage should be chemically well defined and predictable to enable robust structure−function correlations. Additionally, to allow for the grafting of a large diversity of molecular species, the linkage must be formed under mild conditions. Despite this constraint, the linkage must be sufficiently robust to tolerate relatively harsh (electro)catalytic environments. Lastly, in the context of electrocatalysis, the linkage would ideally provide sufficient electronic coupling to the carbon support to enhance electron transfer.

Existing carbon-linkage chemistries are, by and large, unable to satisfy all the above requirements (Scheme 1). Radical grafting methods,[14−16] while controllable in some respects,[17−19] generally lead to a wide diversity of surface connectivity and can introduce undesirable cross reactions with reactive catalytic units. More chemoselective methods exist. For example, triazole connections to carbon can be created via treatment with iodine azide followed by click chemistry with an alkyne and copper catalyst.[20] Additionally, amide linkages can be generated by thionyl chloride treatment of the carbon surface followed by exposure to an amine.[21,22] However, all these methods produce single-point linkages to the carbon surface, which introduce an electron tunneling barrier between the host carbon and the appended molecular unit.[23,24] Aromatic, multipoint linkages can be formed via [4 + 2] cycloaddition of alkynes to carbon edge defects, but the high temperatures (400 °C) required for this chemistry preclude attachment of temperature-sensitive moieties.[25]

One chemical modification strategy stands out with regard to the above criteria. *ortho*-Phenylenediamines condense under mild conditions (e.g., ethanol, 60 °C) with *ortho*-quinone edge defects native to carbon surfaces to create robust aromatic phenazine linkages.[26,27] This facile surface chemistry furnishes a "conjugated" linkage between an appended transition-metal

Received: June 24, 2020
Revised: August 31, 2020
Published: September 1, 2020

https://dx.doi.org/10.1021/acs.chemmater.0c02664
Chem. Mater. 2020, 32, 8512−8521

Scheme 1. Synthetic Strategies for Grafting Molecular Units onto Graphitic Carbon Surfaces

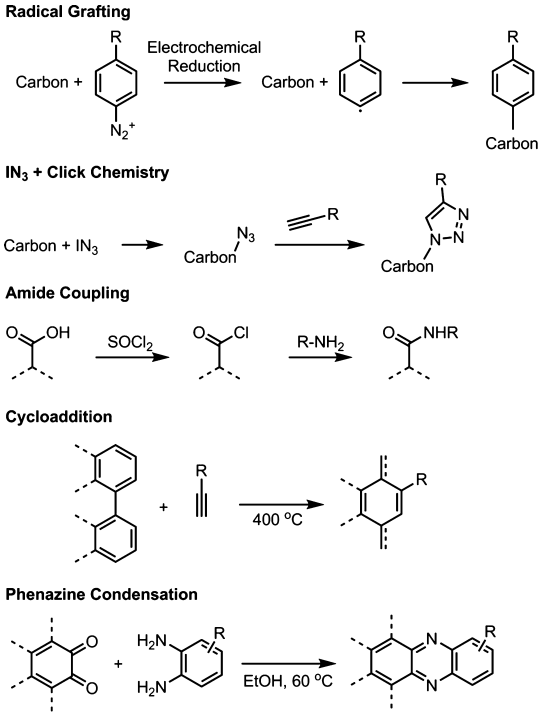

complex and the carbon host. We have shown that graphite conjugation radically alters the mechanism of electron transfer, making the appended unit behave as a metallic active site, rather than an isolated redox-active molecular species.[28,29] Furthermore, Co−porphyrins connected via an aromatic phenazine linkage display an order of magnitude higher catalytic activity for oxygen reduction than those connected to carbon through a simple amide linkage.[30] This change in electrochemical behavior is hypothesized to be due to interaction with the density of states of the bulk carbon and the appended transition-metal site, which embeds the active site within the electrochemical double layer. These promising observations motivate the development of new strategies for forming well-defined heterocyclic linkages to graphitic carbons under mild conditions.

Herein, we expand the synthetic horizons of carbon surface modification by establishing a method for creating imidazole-, pyrimidine-, and imidazopyrimidine-like N-heterocycles on carbon surfaces. These linkages are synthesized by treating carbon surfaces with amidines under basic conditions. We show that oxidic defects from both zigzag and armchair edges on the carbon surface can condense with amidines to form these N-heterocycles, closely following reactivity found for organic molecules (Scheme 2).[31−33] The linkages formed from treating with fluorine-tagged and parent amidines and guanidines (Figure 1) are characterized by a combination of X-ray absorption near-edge structure (XANES) spectroscopy, X-ray photoelectron spectroscopy (XPS), and time-of-flight secondary ion mass spectrometry (TOF-SIMS) tandem mass spectrometry (MS) imaging, which when combined provide an unprecedented level of molecularly precise information about the functionalized carbon surface.

Scheme 2. Condensation of Benzamidine and 2-Aminobenzimidazole to Graphitic Carbon Edge Defects Generates Conjugated Surface Species

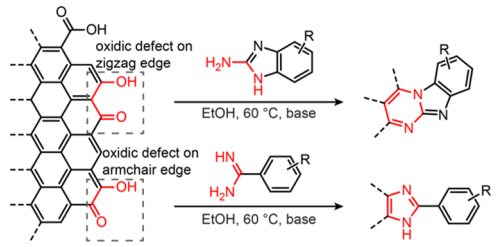

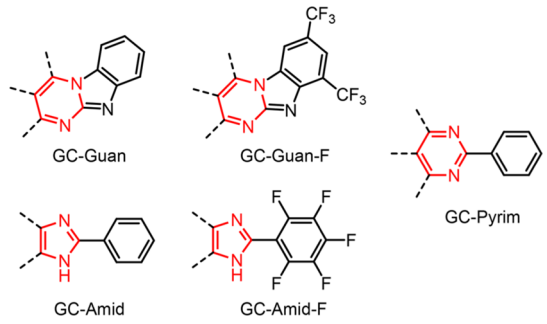

Figure 1. Proposed structures for chemical moieties introduced to the carbon surface.

EXPERIMENTAL SECTION

Materials. Glassy carbon plates were purchased from Goodfellow, and 5 mm OD glassy carbon disk inserts were purchased from Pine Research Instrumentation. Both glassy carbon substrates showed the same behavior and are thus referred to simply as glassy carbon. MONARCH 1300 carbon powder was provided by Cabot Corporation. Synthetic details for precursor molecules are provided in Supporting Information. All aqueous solutions were prepared with reagent grade water (Millipore type 1, 18 MΩ cm resistivity). Concentrated sulfuric acid (ACS grade) was purchased from EMD Millipore.

Carbon Surface Cleaning Procedure. Carbon functionalization was performed on glassy carbon plates, glassy carbon disk inserts, and MONARCH 1300 powder. Glassy carbon plates were anodized by polarizing at +3.5 V versus RHE in a 0.1 M H_2SO_4 solution for 10 s. This anodization treatment serves to increase the quinone functional group population on carbon edge defects[34,35] and remove residual phthalate signals (likely originating from the plastic packaging of the glassy carbon plates) detected in TOF-SIMS measurements. Glassy carbon disk inserts were cleaned prior to each experiment by using a BUEHLER MetaServ 250 grinder-polisher; the disk inserts were slotted into a Teflon holder and placed against a BUEHLER ChemoMet polishing pad with 10 N of force and polished with aqueous 1, 0.3, and 0.05 μm alumina slurries successively for 1 min each. After polishing, glassy carbon disk inserts were anodized by polarizing at +3.5 V versus RHE in a 0.1 M H_2SO_4 solution for 10 s. MONARCH 1300 powder was cleaned before use by Soxhlet extraction in ethanol for 24 h, followed by drying *in vacuo*.

Preparation of Modified Graphitic Surfaces. The graphite-conjugated guanidine (GC-Guan) and amidine (GC-Amid) surfaces were prepared by submerging cleaned carbon in a solution of 2-aminobenzimidazole or benzamidine, respectively, in ethanol with 0.5 equiv of base at 60 °C for 12 h. Afterward, the carbon was soaked in 0.1 M $HClO_4$ for 1 h to remove singly-condensed imine species and physisorbed molecules from the surface and then sonicated in water and ethanol successively to remove any further impurities. Fluorinated versions (GC-Guan-F and GC-Amid-F) were also prepared using the same procedure. These fluorinated samples were particularly useful for the following analyses because fluorine has a higher relative

https://dx.doi.org/10.1021/acs.chemmater.0c02664
Chem. Mater. 2020, 32, 8512−8521

sensitivity factor for XPS than other atoms typically found in organics and is a non-native element to most carbons.

X-Ray Photoelectron Spectroscopy. XPS spectra of glassy carbon and molecular powders were collected using a Physical Electronics PHI VersaProbe II or a Thermo Scientific Nexsa XPS System with hemispherical energy analyzers and monochromatic aluminum K_α X-ray sources (1486.6 eV). Glassy carbon samples were attached to the sample stage with conducting carbon tape. Powder samples were spread out on copper tape, and the copper tape was then affixed to the sample stage using double-sided tape. For glassy carbon and molecular powder samples, data were collected using a 200 μm, 50 W focused X-ray beam at a base pressure of 5×10^{-9} Torr and a take-off angle of 45°. Survey scans were collected with a pass energy of 187.85 eV and a step size of 0.8 eV. High-resolution scans of peaks of interest were collected with a pass energy of 23.50 eV and a step size of 0.1 eV. MONARCH powder sample high-resolution spectra were collected using a 400 μm, 72 W focused X-ray beam at a base pressure $<6 \times 10^{-8}$ Torr, a take-off angle of 90°, a pass energy of 50 eV, and a step size of 0.1 eV. Molecular and carbon powder sample spectra were measured with electron gun and ion gun neutralization. Carbon sample spectra were referenced to the 1s graphitic carbon peak (284.3 eV). Molecular spectra were referenced to the 1s aromatic sp^2 carbon peak (284.3 eV). Data were analyzed with CasaXPS software. Peak fittings were performed with a Shirley-type background and Gaussian/Lorentzian line-shapes with 30% Gaussian shape. Spectra were smoothed using a 5-point quadratic Savitzky–Golay method.

Nitrogen K-Edge XANES. XANES measurements at the N K-edge were performed using beamline 8.0.1 of the advanced light source at Lawrence Berkeley National Laboratory (LBNL).[36] The incident energy resolution of the beamline was set to 0.10 eV at 400 eV. XANES spectra were simultaneously recorded in total electron yield and total fluorescence yield modes by measuring the sample drain current and using a channeltron, respectively. The spectra were normalized to the incident photon flux monitored by measuring the photocurrent produced by an upstream gold mesh. A reference spectrum of hexagonal boron nitride was recorded during the experiment to calibrate the incident photon energy. Samples were pressed into indium foil and oriented at 45° to the incoming beam during measurements. Consecutive spectra from one sample spot were closely monitored for radiation damage, and data were collected at multiple spots on each sample. In all cases, there was no shift in edge energy or change in the spectral profile between consecutive scans, indicating no radiation damage over the scan time.

Infrared Spectroscopy. Attenuated total reflectance infrared (IR) spectra were collected using a Thermo Scientific Nicolet 6700 FT-IR spectrometer and were recorded using a Ge crystal. Carbon powder samples of GC-Amid and GC-Guan were measured at 2 cm^{-1} resolution. The spectral background was collected on MONARCH 1300 powder that had been Soxhlet extracted with ethanol for 24 h.

Raman Spectroscopy. Raman spectra were obtained with an inVia Raman confocal microscope (Renishaw) using a 532 nm laser source at ~5 mW incident power, focused through a 10× objective lens. A 1200 L mm^{-1} holographic reflectance grating was used for dispersion. Spectra were obtained by repetitively scanning the spectral range over 10 s for 10 scans. Baseline subtraction was performed in native Wire software (version 4.4) by fitting the background to a quadratic polynomial.

Time-of-Flight Secondary-Ion Mass Spectrometry. The analyses were performed using a PHI nanoTOF II Parallel Imaging MS/MS instrument (Physical Electronics, Minnesota, USA). A detailed description of this TOF–TOF instrument has been reported previously including the attained spatial resolution, monoisotopic precursor selection, and kiloelectron volt collision-induced dissociation (keV-CID) of the selected precursor ions to generate the tandem MS product ion spectra.[37−39] The elements and qualities of the tandem MS spectra for composition analysis and structure elucidation have been further elaborated in other reports.[40−42] In the present study, all the spectra and images were recorded with electrodynamically bunched pulses of a 30 keV Bi_3^+ primary ion beam of which the DC current was ≈11 nA. The ion beam was operated in the high resolution-squared (HR^2) mode to achieve ≤500 nm lateral resolution at high mass resolving power. The field-of-view of each analytical area was 400 μm × 400 μm divided into 256 × 256 image pixels, that is, each square pixel is 1.56 μm in width and height. TOF-SIMS data were acquired over an m/z range of 0–2000, and the ion fluence (2.18×10^{11} Bi_3^+ cm^{-2}) for each acquisition was at least an order of magnitude below the static limit of analysis. During the analyses, low energy electrons (≤7 eV) and low energy Ar^+ ions (≤10 eV) were applied for charge compensation. Data acquisition was performed using PHI SmartSoft-TOF software, and data processing was performed using the PHI TOF-DR (Physical Electronics, MN) software.

RESULTS AND DISCUSSION

XPS of Modified Carbon Surfaces Reveals Multiple N Environments. XPS measurements of modified glassy carbon surfaces indicate successful functionalization. Survey XPS spectra of GC-Amid-F and GC-Guan-F show an increase in peak intensity in the N 1s region and the appearance of an F 1s peak. For the 2,3,4,5,6-pentafluorobenzamidine-treated sample (GC-Amid-F), the atomic concentration of N and F increased by 2.0 and 5.1%, respectively, in agreement with the expected 2:5 N/F ratio of the precursor molecule. Glassy carbon surfaces functionalized with 5,7-bis(trifluoromethyl)-1*H*-benzo[*d*]imidazol-2-amine (GC-Guan-F) also show an increase in N and F concentration of 2.0 and 2.7%, respectively. Likewise, this ratio is within experimental error of the expected 1:2 ratio found in the precursor compound. For both surfaces, the N atomic concentrations are lower than that generally found for graphite-conjugated phenazines.[27,43] Though GC-Guan and GC-Amid do not display electrochemical redox handles that enable direct quantification of surface sites, we can estimate the surface coverage based on the ratio of XPS atomic concentrations to surface coverage measured electrochemically for graphite-conjugated phenazines (see Supporting Information for details). This rough estimate yields a sub-monolayer coverage of 0.1 nmol cm^{-2} (real surface area basis) for both GC-Guan-F and GC-Amid-F, consistent with functionalization via condensation onto oxygen moieties native to the carbon surface.

High-resolution XPS spectra of the N 1s and F 1s regions reveal local environments about the nitrogen and fluorine atoms consistent with our proposed structures (Figure 2). All binding energies (BEs) are referenced to the graphitic carbon C 1s peak at 284.3 eV. As expected, the F 1s spectra of GC-Amid-F and GC-Guan-F showed BEs matching that of their respective precursor compounds (Figure S1).

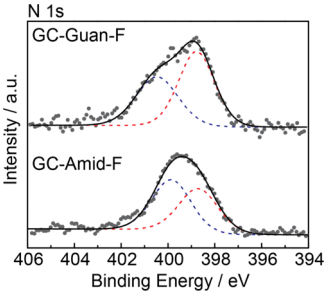

Figure 2. N 1s high-resolution XPS spectra of GC-Guan-F and GC-Amid-F prepared on glassy carbon. Fittings are shown in dashed lines, and the sums of the peak fittings are shown in solid black lines.

https://dx.doi.org/10.1021/acs.chemmater.0c02664
Chem. Mater. 2020, 32, 8512–8521

The N 1s peaks for GC-Guan-F and GC-Amid-F display broad peak envelopes centered at 399.7 and 399.4 eV, respectively. These peak positions are distinct from those of the precursor molecules (Figures S2 and S3), indicating that the nitrogen signal is not from adsorbed precursor species on the surface. For GC-Guan-F, the peak envelope is asymmetric with a shoulder at higher BEs and fits well to two environments corresponding to pyrrolic (blue dashed line) and pyridinic (red dashed line) nitrogens (Figure 2, top) in a 1:2 ratio. This two-peak fit returns full width at half-maximum (fwhm) values of 2.1 and 1.8 eV. For GC-Amid-F, the peak envelope is more symmetric and fits well to pyrrolic (blue dashed line) and pyridinic (red dashed line) nitrogens (Figure 2, bottom) on the surface in a 1:1 ratio. This two-peak fit returns an fwhm of 1.8 eV for both peaks. The observed fwhm for both samples is in line with the range observed previously for graphite conjugated nitrogen moieties of a uniform local structure (Figure S5).[27] Overall, the N 1s XPS data indicate pyrrolic and pyridinic surface nitrogen ratios that agree with the surface linkages shown in Figure 1.

N XANES Measurements Indicate the Presence of Five- and Six-Membered N Heterocyclic Linkages. In order to gather further information of the local nitrogen bonding environment, we performed nitrogen K-edge XANES (N XANES) spectroscopy on GC-Guan (Figure 3i) and GC-Amid (Figure 3v) prepared on MONARCH 1300 carbon powder. Both samples display four distinct resonances at 398.7 (A), 399.7 (B), 401.5 (C), and 402.5 (D) eV. Spectral features between the 398.6 to 405 eV energy range arise from 1s → π^* transitions, whereas broad features with energies greater than 405 eV correspond to 1s → σ^* transitions.[44] Both GC-Amid and GC-Guan show pronounced resonances that lie squarely in the 1s → π^* transition region. Moreover, neither of the samples display the same resonances as their precursor compounds (Figure 3ii,vi). Therefore, both samples have multiple types of nitrogen in π-bonding environments that were not present in their respective precursor compounds.

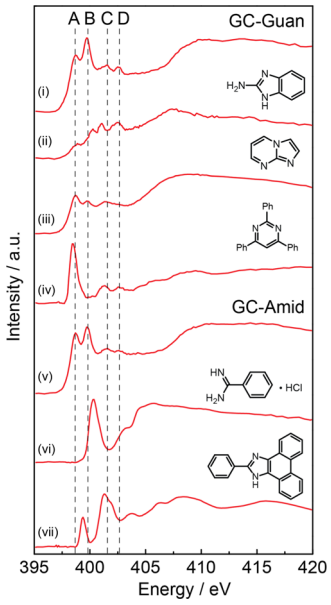

Figure 3. N *K*-edge XANES spectra of (i) GC-Guan, (v) GC-Amid, (ii,vi) precursor compounds, and (iii,iv,vii) model compounds. Four resonance regions are observed for GC-Guan and GC-Amid at 398.7 (A), 399.7 (B), 401.5 (C), and 402.5 (D) eV, consistent with the N-heterocyclic linkages proposed in Figure 1.

These nitrogen 1s → π^* resonance energies can be directly compared to that of other N-heterocyclic compounds. Previous studies on N XANES of N heterocycles have found that the energy of the 1s → π^* transition is largely dependent on the electron density of the nitrogen, which is, in turn, influenced by the local coordination environment.[44,45] Consequently, similar N-heterocycles exhibit similar resonance energies. Peak A, at 398.7 eV, is consistent with 2-coordinate nitrogen species in a six-membered ring, as observed in Figure 3iv. Peak B, at 399.7 eV, has an energy that matches pyridinic, 2-coordinate, nitrogen species in five-membered imidazoles rings such as that observed in Figure 3iii. This peak is slightly positively shifted relative to the peak B at 399.4 eV in 2-aryl-1*H*-phenanthro[9,10-*d*]imidazole (Figure 3vii) but nonetheless falls within the range expected for pyridinic nitrogen in 5-membered rings.[44] Peak C, at 401.5 eV, is line with the energy range expected for pyrrolic, 3-coordinate, nitrogens.[45] Although peak C does also coincide with resonances expected for amide nitrogens, IR spectroscopy (Figures S6 and S7) and TOF-SIMS results (see below) provide no indication of amide linkages on the surface. Notably, the imidazo[1,2-*a*]pyrimidine (Figure 3iii) and 2-aryl-1*H*-phenanthro[9,10-*d*]imidazole (Figure 3vii) both have pyridinic and pyrrolic nitrogens, and they display resonances that correspond to A, B, and C, in varying proportions, supporting our peak assignments. The assignment of peak D is less straightforward. We do not observe this peak in any of our heterocyclic model compounds. However, we note that this peak still falls in the region of pyrrolic nitrogens, and the energy of this peak can be influenced by neighboring surface oxygens that shift π^* resonances to higher energies. While this secondary effect is unaccounted for our model compounds, TOF-SIMS analysis (see below) suggests oxygen moieties in close proximity to the surface linkages and may explain the presence of peak D.

In aggregate, we find that the spectrum of GC-Guan most closely matches that of the imidazo[1,2-*a*]pyrimidine model compound (Figure 3iii) indicating that GC-Guan predominantly forms pyrimidine-like surface connections. In contrast, the spectrum of GC-Amid is best accounted for by a summation of the spectral features observed in the pyrimidine model (Figure 3iv) and pyrrolic model (Figure 3vii), leading us to conclude that GC-Amid forms a combination of imidazole-like and pyrimidine-like surface linkages.

TOF-SIMS Analysis Indicates Pyrimidine Surface Linkages in GC-Guan-F. The data shown so far have only addressed the local environment of the nitrogens present on the modified carbon samples. By performing TOF-SIMS tandem MS imaging, we obtained molecular-level structural information of the local binding environment of the surface linkages themselves. TOF-SIMS tandem MS imaging was performed by bombarding a modified carbon sample surface with Bi_3^+ clusters and examining the secondary ions liberated from the surface. We used carbon surfaces modified with fluorinated precursors to introduce easily identifiable F atoms into the tandem MS product ion (MS^2) spectra. The MS^1 spectra were calibrated using three ions at low mass-to-charge ratio (m/z), C_2H^- (m/z 25.0078), C_4H^- (m/z 49.0078), and $C_2H_2O_2^-$ (m/z 58.0054) in the negative channel. This method provides sufficient mass accuracy for monoisotopic precursor selection and generation of the associated MS^2 spectra. The

https://dx.doi.org/10.1021/acs.chemmater.0c02664
Chem. Mater. 2020, 32, 8512−8521

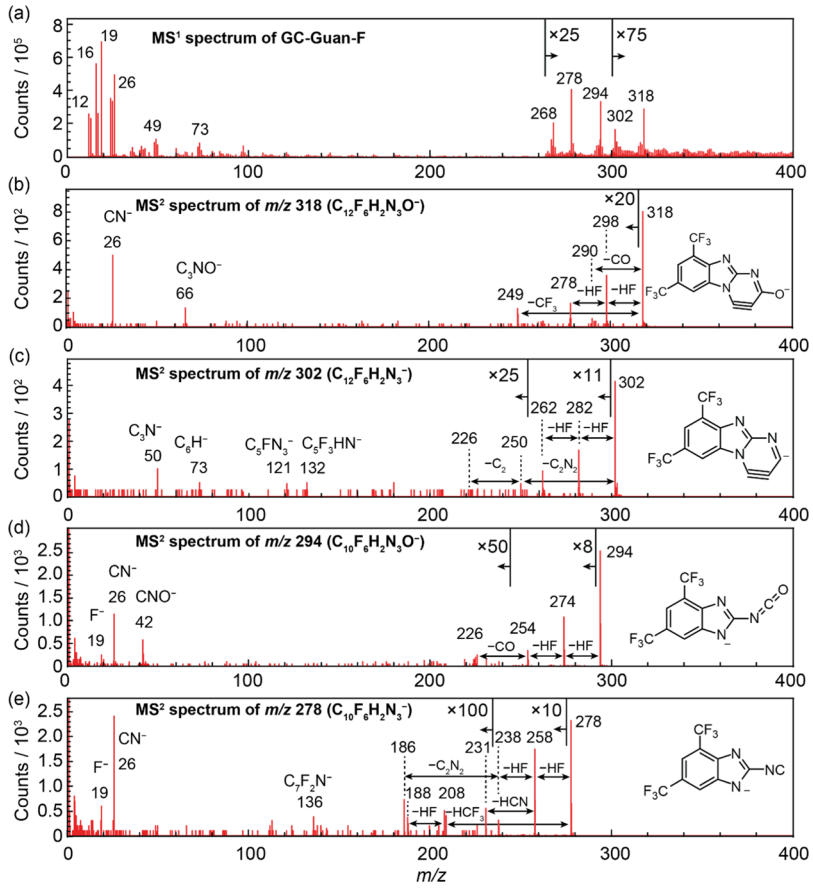

Figure 4. (a) Negative ion polarity TOF-SIMS (MS^1) spectrum of GC-Guan-F. Tandem MS product ion (MS^2) spectra of precursor ions arising at m/z (b) 318, (c) 302, (d) 294, and (e) 278 are shown with putative structural assignments. Sections of each spectra are magnified to show relevant peaks. Assignments for prominent neutral losses are indicated by arrows between two peaks. For each MS^2 spectrum, the accuracy of the precursor ion composition is based on the confidence provided by the calculated mass accuracy ($\Delta_{m/z}$). The calculated $\Delta_{m/z}$ is (b) −5.95 ppm, (c) +5.44 ppm, (d) −6.97 ppm, and (e) −8.12 ppm.

MS^2 spectra were calibrated as described elsewhere for precursor and product ion attributions.[39−42]

The MS^1 spectrum of GC-Guan-F displays the diversity of secondary ions generated from Bi_3^+ bombardment (Figure 4a). Notable peaks across the m/z scale that ostensibly originate from the GC-Guan-F chemical structure have been highlighted. The surface has a readily observed abundance of fluoride (F^-, m/z 19), cyanide (CN^-, m/z 26), and larger mass fragments that can be traced to the introduced guanidine molecule. Prominent high m/z peaks are found at 268, 278, 294, 302, and 318. The peak at m/z 268 corresponds to free precursor, which likely arises from trace aminobenzimidazole physisorbed on the glassy carbon surface.

Kiloelectron volt collision-induced dissociation (keV-CID) of the prominent high m/z ions produces MS^2 spectra (Figure 4b−e) that enable their structural assignments. In all cases, MS^2 spectra display successive loss of HF (20 Dalton, Da) which is expected to arise from collision-induced coupling of H atoms on the aromatic ring and F atoms from the $-CF_3$ group. Notably, product ions that have already lost two HF molecules do not undergo further HF losses, as exemplified by the MS^2 spectrum of the m/z 238 precursor ion (Figure S13). In addition, for the m/z 318 precursor ion, we also observe loss of a $-CF_3$ group. Given the negligible F content of the carbon, these losses indicate that all selected precursor ions result from the aminobenzimidazole condensate.

The MS^2 spectra provide precise information about the structure of the surface linkages in GC-Guan-F. For the m/z 318 precursor ion, we observe loss of CO (28 Da) and the appearance of CN^- (m/z 26) and C_3NO^- (m/z 66) product ions. The C_3NO^- product ion and the neutral CO loss are indicative of an oxygen atom in the precursor ion. Because the 2-aminobenzimidazole precursor contains no oxygens, this data indicates that an oxygen atom exists in the local environment of the surface linkage. Taken together, the MS^2 fragmentation pattern is most consistent with the structure inset in Figure 4b. Such a structure could be formed on a carbon surface by condensation of 2-aminobenzimidazole to a β-ketolactone-like moiety on carbon, as shown in Scheme 3. Similar analyses were performed on precursor ions m/z 302, 294, and 278 (Figure 4c−e), which indicate that they are all structurally related to the m/z 318 precursor ion discussed above. In particular, the MS^2 spectra of the m/z 294 precursor ion (Figure 4d) showed

Scheme 3. Reaction of a β-Ketolactone-like Moiety on the Carbon Surface and 2-Aminobenzimidazole

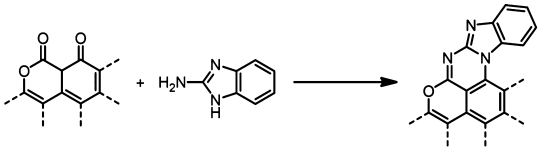

https://dx.doi.org/10.1021/acs.chemmater.0c02664
Chem. Mater. 2020, 32, 8512−8521

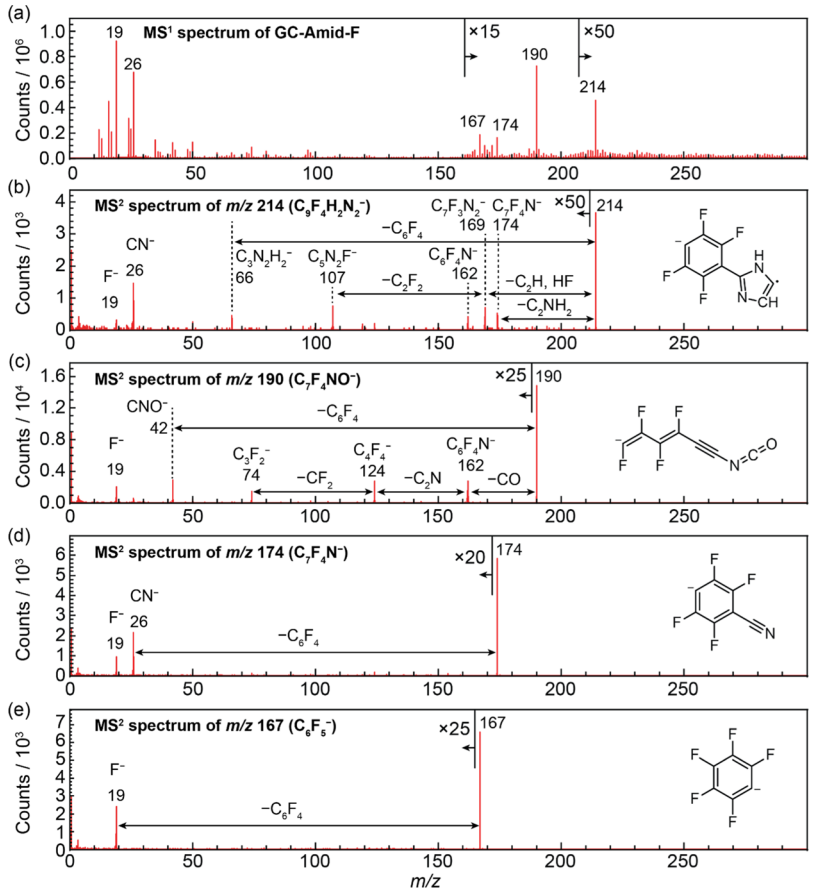

Figure 5. (a) Negative ion polarity TOF-SIMS (MS^1) spectrum of GC-Amid-F. Tandem MS product ion (MS^2) spectra of precursor ions arising from m/z (b) 214, (c) 190, (d) 174, and (e) 167 are shown with their putative structural assignments. Sections of each spectra are magnified to show relevant peaks. Assignments for prominent neutral losses are indicated by arrows between two peaks. For each MS^2 spectrum, the accuracy of the precursor ion composition is based on the confidence provided by the calculated mass accuracy ($\Delta_{m/z}$). The calculated $\Delta_{m/z}$ values are (b) +8.99 ppm, (c) +1.87 ppm, and (d) +7.11 ppm. The mass accuracy could not be calculated for (e) using only the precursor ion and the F^- product ion.

CNO^- (m/z 42) and CO (28 Da) loss, indicating the presence of oxygen, and a simple subtraction of a C_2 unit from the structure in Figure 4b inset produced a viable structural candidate (Figure 4d inset). The m/z 302 and 278 precursor ions do not display characteristic oxygen losses, and their masses correspond to the removal O and C_2O units, respectively, relative to the m/z 318 precursor ion. Further analysis of the associated neutral losses and product ions is provided in Table S1 and supports the structural assignments in the insets of Figure 4c−e. In summary, the MS^2 data provide strong evidence of pyrimidine linkages on the surface of GC-Guan-F that are formed by condensation with β-ketoenol and β-ketolactone moieties on zigzag edges of the graphitic carbon.

Following the assignment of the ion compositions on the MS^2 spectra of GC-Guan-F, we performed spectral calibrations based on our assignments to further substantiate the precursor and product ion attributions. The calibrations provided both the calculated mass accuracy ($\Delta_{m/z}$) at the precursor ion (reported in units of ppm below) and the average accuracy of all MS^2 product peaks used in the calibration (reported in units of ppm ave.); both are measures of the correctness for the peak compositions. The precursor ions at m/z 318 ($C_{12}F_6H_2N_3O^-$), 302 ($C_{12}F_6H_2N_3^-$), 294 ($C_{10}F_6H_2N_3O^-$), and 278 ($C_{10}F_6H_2N_3^-$) have mass accuracies of −5.95 ppm (+1.76 ppm ave.), +5.44 ppm (+0.55 ppm ave.), −6.97 ppm (+2.77 ppm ave.), and −8.12 ppm (+2.85 ppm ave.), respectively. Most of the product ions had a signal-to-background ratio (S/B) < 20, wherein the peak centroid was ill-defined; this contributed to the high calculated $\Delta_{m/z}$. (Typically, $\Delta_{m/z} > \pm 2$ ppm represents diminishing confidence.) Nevertheless, reasonable mass accuracies were achieved, and the collective weight of the data supports both the peak compositions and the proposed structures.

Precursor ions with larger m/z also showed evidence for guanidine linkages on GC-Guan-F. The precursor ions at m/z 693 and 665 (Figures S11 and S12) exhibited dissociation into product ions m/z 278 and 665 and 278, 302, and 318, respectively. Although exact chemical compositions of the m/z 693 and 665 precursor ions cannot be determined with the available data, these data both demonstrate that Bi_3^+ bombardment liberates larger carbon fragments that also contain the surface-condensed guanidine moiety as a substructure. MS^2 spectra of m/z < 250 precursor ions were also collected and analyzed. Selected MS^2 spectra that likely originated from GC-Guan-F are shown in Figures S13−S17. Taken together, the TOF-SIMS data point strongly to pyrimidine surface linkages on zigzag edges present in GC-Guan-F.

TOF-SIMS Analysis Indicates Imidazole Linkages in GC-Amid-F. We performed a similar analysis on the secondary

https://dx.doi.org/10.1021/acs.chemmater.0c02664
Chem. Mater. 2020, 32, 8512−8521

anions arising from the GC-Amid-F surface (Figure 5). In addition to the expected F^- (m/z 19) and CN^- (m/z 26) peaks at low m/z, these measurements showed high mass peaks at m/z 167, 174, 190, and 214 (Figure 5a). Notably, for the GC-Amid-F, we do not observe any appreciable peak at m/z 209 or 210 that would correspond to the anion of the adsorbed molecular benzamidine precursor.

All of the prominent high mass peaks further fragment to reveal F^- in the MS^2 spectra (Figure 5b–d), indicating that they all arise from the surface bound GC-Amid-F moieties. Among these high mass peaks, the m/z 167 precursor ion displayed the simplest MS^2 spectrum (Figure 5e), with loss of the C_6F_4 (148 Da) neutral fragment. This leads to straightforward assignment of this peak as $C_6F_5^-$, as depicted in Figure 5e inset. Similarly, the m/z 174 precursor ion displays loss of the same C_6F_4 neutral fragment to reveal the CN^- ion in the MS^2 spectrum (Figure 5d). Thus, we assign this peak to the $C_6F_4CN^-$ ion (Figure 5d inset).

The precursor ion m/z 190 is 16 Da greater than m/z 174 and exhibited a neutral loss of CO (28 Da), compellingly suggesting the presence of an oxygen atom that may originate from a carbon surface lactone (Figure S18). There were also product ions with S/B ≥ 8 at m/z 50 (C_3N^-), 74 ($C_3F_2^-$), and 124 ($C_6F_4N^-$). Additionally, the MS^2 spectrum of m/z 190 revealed successive losses with strong intensity, as opposed to the orthogonal losses that are observed in many of the other MS^2 spectra in Figures 4 and 5. Such successive losses with high S/B are commonly observed in linear molecules.[40] Therefore, we assigned the m/z 190 precursor ion to a ring-opened structure, as shown in Figure 5c.

The MS^2 spectrum of the m/z 214 precursor ion reveals that GC-Amid-F contains an imidazole-like five-membered ring (Figure 5b). Indeed, the m/z 66 ($C_3N_2H_2^-$) peak corresponds to an intact imidazole product ion. While the m/z 66 peak would also be consistent with an oxazole-like ring (C_3NO^-), that assignment requires a complex array of fragmentation/rearrangement reactions to explain the other product ions. In contrast, the assignment of m/z 66 as an imidazole product ion is consistent with successive neutral losses of HF, C_2H, and C_2F_2 that produces the m/z 107 peak (Figure S19). Notably, evidence for the formation of a six-membered pyrimidine-like ring was not observed from TOF-SIMS measurements on GC-Amid-F.

As described above for the GC-Guan-F MS^2 spectra, we performed spectral calibrations on our GC-Amid-F MS^2 spectra to further appraise the accuracy of our precursor and product ion attributions. In the case of the precursor ions at m/z 214 ($C_9F_4N_2H_2^-$), 190 ($C_7F_4NO^-$), and 174 ($C_7F_4N^-$), the calculated mass accuracies were +8.99 ppm (+12.46 ppm ave.), +1.89 ppm (−11.07 ppm ave.), and +7.11 ppm (+8.08 ppm ave.), respectively. These peak accuracies are very much in line with expectation, particularly given the low S/B < 20 of many of the product ions, which impedes precise fitting of the peak centroids. We note that mass accuracies could not be determined for the m/z 167 ion because of the relatively few product ions available for mass calibration. Nonetheless, this mass accuracy analysis supports our chemical formula assignments of the precursor ions. Together, the TOF-SIMS analysis provides strong evidence for the presence of imidazole surface linkages in GC-Amid-F.

DISCUSSION

Here, we have used a combination of XPS, N XANES, and TOF-SIMS to characterize, at a molecular level, surface linkages that are formed from treatment of graphitic carbon surfaces with amidine and guanidine precursors. These studies revealed that GC-Guan selectively forms surface pyrimidine linkages, whereas GC-Amid forms both pyrimidine and imidazole linkages, in varying ratios, depending on the substitution pattern of the amidine precursor.

The foregoing conclusions relied on the high structure sensitivity of N XANES in combination with the molecularly precise information provided by TOF-SIMS tandem MS analysis. In particular, N XANES spectra capture the diversity of local N environments but provide limited information about the extended connectivity of the surface linkage. On the other hand, TOF-SIMS analysis of relatively large molecular fragments provides unique insights into longer range connectivity but is unable to sample all environments with equal sensitivity. Importantly, the coupling of TOF-SIMS with tandem MS was critical for unambiguous structural assignments. Together, this work highlights the value of multi-technique analysis for characterizing novel carbon surface chemistry with exceptional molecular precision.

We build on previous studies that have also characterized modified carbon surfaces using TOF-SIMS. One such study focused on the change in functional groups on carbon fibers after chemical treatment by examining small secondary ions (m/z < 100) originating from carbon fibers.[46,47] Another set of papers probe the catalytic activity of pyrolyzed Co/N/C catalysts via TOF-SIMS by using either CN^- or $CoN_xC_z^+$ ion fragments as proxies for the surface concentration of catalytic sites.[48,49] In contrast to these examples, we focus on secondary ions that have similar or larger m/z than the precursor amidine and guanidine molecules. In our samples, these larger secondary ions cannot originate from the physisorbed precursor and instead must arise from covalently bonded moieties. A similar approach was demonstrated in a study on polymeric films grafted onto carbon surfaces, which found ion fragments suggesting a polymer−C_2−OH linkage, where the C_2OH was proposed to have originated from a phenolic group on the carbon surface.[15,16] Our tandem MS analysis lets us take one step further and make detailed structural assignments of complex, multibond aromatic linkages. Thus, our work expands the breadth of analysis possible by TOF-SIMS.

The structural insights that emerge from this study establish that the selectivity of the surface linkage can be controlled by tuning the structure of the precursor molecule. In particular, the reactivity patterns of the graphitic carbon surface follow basic principles of physical organic chemistry. For example, the more nucleophilic benzamidine undergoes condensation at both the zigzag and armchair oxidic functional groups to generate both pyrimidine and imidazole linkages in GC-Amid. In contrast, the less nucleophilic 2,3,4,5,6-pentafluorobenzamidine shows a preference for condensation with more electrophilic *ortho*-quinone structures found on armchair edges of graphitic carbon, forming predominantly imidazole linkages in GC-Amid-F. On the other hand, by using a precursor guanidine bound in a 5-membered ring, such as 2-aminobenzimidazole or 5,7-bis(trifluoromethyl)-1*H*-benzo[*d*]-imidazol-2-amine, one can steer the surface linkage toward the less-electrophilic β-ketoenol functional groups prevalent on the zigzag edges to form pyrimidine linkages with high selectivity.

https://dx.doi.org/10.1021/acs.chemmater.0c02664
Chem. Mater. 2020, 32, 8512−8521

The lack of significant surface imidazole linkages on GC-Guan is attributed to the sizable strain inherent in the formation of a 5−5 fused ring system. Together, these results indicate that ring structure and nucleophilicity of a precursor molecule are powerful handles for guiding the selectivity of surface condensation reactions (Scheme 4).

Scheme 4. Summary of Possible Reactions of Amidines and Carbon Surface Oxidic Edge Defects

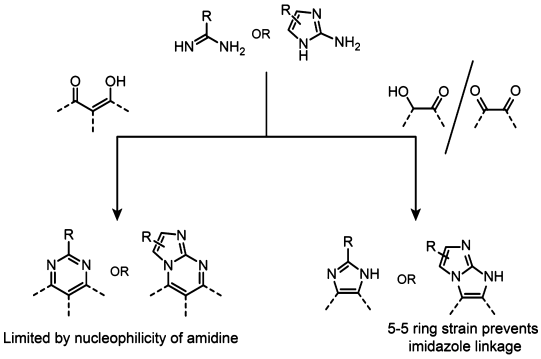

The high-fidelity linkage chemistries demonstrated in this paper, GC-Amid and GC-Guan, enable a significant expansion of the (electro)catalytic chemistry of chemically modified carbons. The nature of the surface linkage sets the barrier to electron flow between the carbon and the appended molecular unit and can even radically alter the mechanism of electron transfer.[28,29] Furthermore, the electronic structures of the zigzag and armchair edges are dramatically distinct, and thus, selective ligation to one edge over the other could uncover unique catalytic behavior.[50] Lastly, the expansion of the surface linkage chemistry provided here enables the creation of multifunctional carbons with spatially isolated, electronically connected active sites that could act in concert to carry out demanding thermal and electrochemical transformations.[22,51]

CONCLUSIONS

We establish that condensing amidine-containing compounds with graphitic carbon surfaces generates well-defined pyrimidine and imidazole linkages to native edge defects. XPS, N XANES, and TOF-SIMS tandem MS analysis provide corroborating evidence that the acyclic amidine precursor molecules form both pyrimidine and imidazole linkages depending on the nucleophilicity of the precursor. In contrast, the data evince selective formation of pyrimidine linkages upon surface condensation with a 5-membered cyclic guanidine precursor. This work showcases the combination of multiple analytical techniques to characterize sub-monolayer surface linkage chemistry with molecular-level detail, despite the complex heterogeneity inherent to carbon surfaces.

ASSOCIATED CONTENT

Supporting Information

The Supporting Information is available free of charge at https://pubs.acs.org/doi/10.1021/acs.chemmater.0c02664.

Synthetic details and XPS, IR, Raman, and TOF-SIMS spectra (PDF)

AUTHOR INFORMATION

Corresponding Authors

Gregory L. Fisher − *Physical Electronics, Inc., Chanhassen, Minnesota 55317, United States;* orcid.org/0000-0001-7517-0512; Email: gfisher@phi.com

Yogesh Surendranath − *Department of Chemistry, Massachusetts Institute of Technology, Cambridge, Massachusetts 02139, United States;* orcid.org/0000-0003-1016-3420; Email: yogi@mit.edu

Authors

Seokjoon Oh − *Department of Chemistry, Massachusetts Institute of Technology, Cambridge, Massachusetts 02139, United States;* orcid.org/0000-0002-8980-5213

Ryan P. Bisbey − *Department of Chemistry, Massachusetts Institute of Technology, Cambridge, Massachusetts 02139, United States*

Sheraz Gul − *Molecular Biophysics and Integrated Bioimaging Division, Lawrence Berkeley National Laboratory, Berkeley, California 94720, United States;* orcid.org/0000-0001-8920-8737

Junko Yano − *Molecular Biophysics and Integrated Bioimaging Division, Lawrence Berkeley National Laboratory, Berkeley, California 94720, United States;* orcid.org/0000-0001-6308-9071

Complete contact information is available at: https://pubs.acs.org/10.1021/acs.chemmater.0c02664

Author Contributions

S.O. and Y.S. conceived of the study. S.O. synthesized samples and analyzed all results. G.L.F. contributed to TOF-SIMS experimental details and analysis. S.G. and J.Y. provided experimental details for XANES measurements. S.O. and Y.S. composed the manuscript. R.P.B. replicated synthetic methods and performed spectroscopy of carbon powders.

Notes

The authors declare no competing financial interest.

ACKNOWLEDGMENTS

We acknowledge Alexander T. Murray for providing assistance in synthesizing amidines as potential graphite-conjugated catalyst precursors. This research was supported by the Department of Energy, Office of Science, Office of Basic Energy Sciences, Catalysis Science Program, under award DE-SC0020973. S.O. was supported by the National Science Foundation Graduate Research Fellowship under grant no. 1122374. This work made use of the MRSEC Shared Experimental Facilities at MIT, supported by the National Science Foundation under award no. DMR-1419807. This work was performed in part at the Center for Nanoscale Systems (CNS), a member of the National Nanotechnology Coordinated Infrastructure Network (NNCI), which is supported by the National Science Foundation under NSF award no. 1541959. CNS is part of Harvard University. The XANES data were collected at the advanced light source, BL 8.0.1, in collaboration with the Joint Center for Artificial Photosynthesis, a DOE Energy Innovation Hub, supported through the Office of Science of the U.S. Department of Energy (award no. DE-SC0004993). This research used resources of the advanced light source, which is a DOE Office of Science User Facility under contract no. DE-AC02-05CH11231.

https://dx.doi.org/10.1021/acs.chemmater.0c02664
Chem. Mater. 2020, 32, 8512−8521

REFERENCES

(1) Cameron, D. S.; Cooper, S. J.; Dodgson, I. L.; Harrison, B.; Jenkins, J. W. Carbons as supports for precious metal catalysts. *Catal. Today* **1990**, *7*, 113−137.

(2) Stiles, A. B. *Catalyst Supports and Supported Catalysts*; Butterworths: Boston, 1987.

(3) Uen, T.; Kushiro, K.; Hibino, H.; Takai, M. Surface functionalization of carbon-based sensors with biocompatible polymer to enable electrochemical measurement in protein-rich environment. *Sens. Actuators, B* **2020**, *309*, 127758.

(4) Li, M.; Lu, J.; Chen, Z.; Amine, K. 30 Years of Lithium-Ion Batteries. *Adv. Mater.* **2018**, *30*, 1800561.

(5) Wu, J.; Lan, Z.; Lin, J.; Huang, M.; Huang, Y.; Fan, L.; Luo, G.; Lin, Y.; Xie, Y.; Wei, Y. Counter electrodes in dye-sensitized solar cells. *Chem. Soc. Rev.* **2017**, *46*, 5975−6023.

(6) Borenstein, A.; Hanna, O.; Attias, R.; Luski, S.; Brousse, T.; Aurbach, D. Carbon-based composite materials for supercapacitor electrodes: a review. *J. Mater. Chem. A* **2017**, *5*, 12653−12672.

(7) Zolochevsky, A.; Hop, J. G.; Servant, G.; Foosnæs, T.; Øye, H. A. Rapoport−Samoilenko test for cathode carbon materials: I. Experimental results and constitutive modelling. *Carbon* **2003**, *41*, 497−505.

(8) Dicks, A. L. The role of carbon in fuel cells. *J. Power Sources* **2006**, *156*, 128−141.

(9) Dombrovskis, J. K.; Palmqvist, A. E. C. Recent Progress in Synthesis, Characterization and Evaluation of Non-Precious Metal Catalysts for the Oxygen Reduction Reaction. *Fuel Cells* **2016**, *16*, 4−22.

(10) Kong, X.-K.; Chen, C.-L.; Chen, Q.-W. Doped graphene for metal-free catalysis. *Chem. Soc. Rev.* **2014**, *43*, 2841−2857.

(11) Zhao, S.; Wang, D.-W.; Amal, R.; Dai, L. Carbon-Based Metal-Free Catalysts for Key Reactions Involved in Energy Conversion and Storage. *Adv. Mater.* **2018**, *31*, 1801526.

(12) Navalon, S.; Dhakshinamoorthy, A.; Alvaro, M.; Garcia, H. Carbocatalysis by Graphene-Based Materials. *Chem. Rev.* **2014**, *114*, 6179−6212.

(13) Radovic, L. R.; Rodriguez-Reinoso, F. Carbon Materials in Catalysis. In *Chemistry and Physics of Carbon*; Thrower, P. A., Ed.; Marcel Dekker: New York, 1997; Vol. 25, pp 276−312.

(14) Allongue, P.; Delamar, M.; Desbat, B.; Fagebaume, O.; Hitmi, R.; Pinson, J.; Savéant, J.-M. Covalent Modification of Carbon Surfaces by Aryl Radicals Generated from the Electrochemical Reduction of Diazonium Salts. *J. Am. Chem. Soc.* **1997**, *119*, 201−207.

(15) Combellas, C.; Kanoufi, F.; Pinson, J.; Podvorica, F. I. Time-of-Flight Secondary Ion Mass Spectroscopy Characterization of the Covalent Bonding between a Carbon Surface and Aryl Groups. *Langmuir* **2005**, *21*, 280−286.

(16) Doppelt, P.; Hallais, G.; Pinson, J.; Podvorica, F.; Verneyre, S. Surface Modification of Conducting Substrates. Existence of Azo Bonds in the Structure of Organic Layers Obtained from Diazonium Salts. *Chem. Mater.* **2007**, *19*, 4570−4575.

(17) Bélanger, D.; Pinson, J. Electrografting: a powerful method for surface modification. *Chem. Soc. Rev.* **2011**, *40*, 3995−4048.

(18) Leroux, Y. R.; Fei, H.; Noël, J.-M.; Roux, C.; Hapiot, P. Efficient Covalent Modification of a Carbon Surface: Use of a Silyl Protecting Group To Form an Active Monolayer. *J. Am. Chem. Soc.* **2010**, *132*, 14039−14041.

(19) Zhang, Y.; Tamijani, A. A.; Taylor, M. E.; Zhi, B.; Haynes, C. L.; Mason, S. E.; Hamers, R. J. Molecular Surface Functionalization of Carbon Materials via Radical-Induced Grafting of Terminal Alkenes. *J. Am. Chem. Soc.* **2019**, *141*, 8277−8288.

(20) Devadoss, A.; Chidsey, C. E. D. Azide-Modified Graphitic Surfaces for Covalent Attachment of Alkyne-Terminated Molecules by "Click" Chemistry. *J. Am. Chem. Soc.* **2007**, *129*, 5370−5371.

(21) Stein, A.; Wang, Z.; Fierke, M. A. Functionalization of Porous Carbon Materials with Designed Pore Architecture. *Adv. Mater.* **2009**, *21*, 265−293.

(22) Chu, S. B.; Fukushima, T.; Surendranath, Y. Minor Impact of Ligand Shell Steric Profile on Colloidal Nanocarbon Catalysis. *Chem. Mater.* **2017**, *29*, 495−498.

(23) Zhang, L.; Vilà, N.; Kohring, G.-W.; Walcarius, A.; Etienne, M. Covalent Immobilization of (2,2′-Bipyridyl) (Pentamethylcyclopentadienyl)-Rhodium Complex on a Porous Carbon Electrode for Efficient Electrocatalytic NADH Regeneration. *ACS Catal.* **2017**, *7*, 4386−4394.

(24) Tong, L.; Göthelid, M.; Sun, L. Oxygen evolution at functionalized carbon surfaces: a strategy for immobilization of molecular water oxidation catalysts. *Chem. Commun.* **2012**, *48*, 10025−10027.

(25) Ssenyange, S.; Anariba, F.; Bocian, D. F.; McCreery, R. L. Covalent Bonding of Alkene and Alkyne Reagents to Graphitic Carbon Surfaces. *Langmuir* **2005**, *21*, 11105−11112.

(26) Thorogood, C. A.; Wildgoose, G. G.; Crossley, A.; Jacobs, R. M. J.; Jones, J. H.; Compton, R. G. Differentiating between ortho- and para-Quinone Surface Groups on Graphite, Glassy Carbon, and Carbon Nanotubes Using Organic and Inorganic Voltammetric and X-ray Photoelectron Spectroscopy Labels. *Chem. Mater.* **2007**, *19*, 4964−4974.

(27) Oh, S.; Gallagher, J. R.; Miller, J. T.; Surendranath, Y. Graphite-Conjugated Rhenium Catalysts for Carbon Dioxide Reduction. *J. Am. Chem. Soc.* **2016**, *138*, 1820−1823.

(28) Jackson, M. N.; Oh, S.; Kaminsky, C. J.; Chu, S. B.; Zhang, G.; Miller, J. T.; Surendranath, Y. Strong Electronic Coupling of Molecular Sites to Graphitic Electrodes via Pyrazine Conjugation. *J. Am. Chem. Soc.* **2018**, *140*, 1004−1010.

(29) Jackson, M. N.; Kaminsky, C. J.; Oh, S.; Melville, J. F.; Surendranath, Y. Graphite Conjugation Eliminates Redox Intermediates in Molecular Electrocatalysis. *J. Am. Chem. Soc.* **2019**, *141*, 14160−14167.

(30) Kaminsky, C. J.; Wright, J.; Surendranath, Y. Graphite-Conjugation Enhances Porphyrin Electrocatalysis. *ACS Catal.* **2019**, *9*, 3667−3671.

(31) Kulisch, V. Zur Kenntniss des Lophins und der Glyoxaline. *Monatsh. Chem.* **1896**, *17*, 300−308.

(32) Künstlinger, M.; Breitmaier, E. Imidazo[1,2-a]pyrimidine aus 2-Aminoimidazolen und 3-Alkoxyacroleinen. *Synthesis* **1983**, 161−162.

(33) Fandrick, D. R.; Reinhardt, D.; Desrosiers, J.-N.; Sanyal, S.; Fandrick, K. R.; Ma, S.; Grinberg, N.; Lee, H.; Song, J. J.; Senanayake, C. H. General and Rapid Pyrimidine Condensation by Addressing the Rate Limiting Aromatization. *Org. Lett.* **2014**, *16*, 2834−2837.

(34) McDermott, C. A.; Kneten, K. R.; McCreery, R. L. Electron Transfer Kinetics of Aquated $Fe^{+3/+2}$, $Eu^{+3/+2}$, and $V^{+3/+2}$ at Carbon Electrodes: Inner Sphere Catalysis by Surface Oxides. *J. Electrochem. Soc.* **2019**, *140*, 2593−2599.

(35) McCreery, R. L. Advanced Carbon Electrode Materials for Molecular Electrochemistry. *Chem. Rev.* **2008**, *108*, 2646−2687.

(36) Warwick, T.; Heimann, P.; Mossessian, D.; McKinney, W.; Padmore, H. Performance of a high resolution, high flux density SGM undulator beamline at the ALS (invited). *Rev. Sci. Instrum.* **1995**, *66*, 2037−2040.

(37) Fisher, G. L.; Bruinen, A. L.; Ogrinc Potočnik, N.; Hammond, J. S.; Bryan, S. R.; Larson, P. E.; Heeren, R. M. A. A New Method and Mass Spectrometer Design for TOF-SIMS Parallel Imaging MS/MS. *Anal. Chem.* **2016**, *88*, 6433−6440.

(38) Fisher, G. L.; Hammond, J. S.; Bryan, S. R.; Larson, P. E.; Heeren, R. M. A. The Composition of Poly(Ethylene Terephthalate) (PET) Surface Precipitates Determined at High Resolving Power by Tandem Mass Spectrometry Imaging. *Microsc. Microanal.* **2017**, *23*, 843−848.

(39) Chini, C. E.; Fisher, G. L.; Johnson, B.; Tamkun, M. M.; Kraft, M. L. Observation of endoplasmic reticulum tubules via TOF-SIMS tandem mass spectrometry imaging of transfected cells. *Biointerph* **2018**, *13*, 03B409.

(40) Fu, T.; Touboul, D.; Della-Negra, S.; Houël, E.; Amusant, N.; Duplais, C.; Fisher, G. L.; Brunelle, A. Tandem Mass Spectrometry Imaging and in Situ Characterization of Bioactive Wood Metabolites

https://dx.doi.org/10.1021/acs.chemmater.0c02664
Chem. Mater. 2020, 32, 8512−8521

in Amazonian Tree Species Sextonia rubra. *Anal. Chem.* **2018**, *90*, 7535−7543.
(41) Fu, T.; Houël, E.; Amusant, N.; Touboul, D.; Genta-Jouve, G.; Della-Negra, S.; Fisher, G. L.; Brunelle, A.; Duplais, C. Biosynthetic investigation of γ-lactones in Sextonia rubra wood using in situ TOF-SIMS MS/MS imaging to localize and characterize biosynthetic intermediates. *Sci. Rep.* **2019**, *9*, 1928.
(42) Shi, Y.; Johnson, J.; Wang, B.; Chen, B.; Fisher, G. L.; Urabe, G.; Shi, X.; Kent, K. C.; Guo, L.-W.; Li, L. Mass Spectrometric Imaging Reveals Temporal and Spatial Dynamics of Bioactive Lipids in Arteries Undergoing Restenosis. *J. Proteome Res.* **2019**, *18*, 1669−1678.
(43) Fukushima, T.; Drisdell, W.; Yano, J.; Surendranath, Y. Graphite-Conjugated Pyrazines as Molecularly Tunable Heterogeneous Electrocatalysts. *J. Am. Chem. Soc.* **2015**, *137*, 10926−10929.
(44) Leinweber, P.; Kruse, J.; Walley, F. L.; Gillespie, A.; Eckhardt, K.-U.; Blyth, R. I. R.; Regier, T. Nitrogen K-edge XANES − an overview of reference compounds used to identify 'unknown' organic nitrogen in environmental samples. *J. Synchrotron Radiat.* **2007**, *14*, 500−511.
(45) Mullins, O. C.; Mitra-Kirtley, S.; Van Elp, J.; Cramer, S. P. Molecular Structure of Nitrogen in Coal from XANES Spectroscopy. *Appl. Spectrosc.* **1993**, *47*, 1268−1275.
(46) Alexander, M. R.; Jones, F. R. Effect of electrolytic oxidation upon the surface chemistry of type A carbon fibres—Part II, analysis of derivatised surface functionalities by XPS, and TOF SIMS. *Carbon* **1995**, *33*, 569−580.
(47) Alexander, M. R.; Jones, F. R. Effect of electrolytic oxidation upon the surface chemistry of type A carbon fibres: III. Chemical state, source and location of surface nitrogen. *Carbon* **1996**, *34*, 1093−1102.
(48) Weng, L. T.; Bertrand, P.; Lalande, G.; Guay, D.; Dodelet, J. P. Surface characterization by time-of-flight SIMS of a catalyst for oxygen electroreduction: pyrolyzed cobalt phthalocyanine-on-carbon black. *Appl. Surf. Sci.* **1995**, *84*, 9−21.
(49) Lefèvre, M.; Dodelet, J. P.; Bertrand, P. Molecular Oxygen Reduction in PEM Fuel Cell Conditions: ToF-SIMS Analysis of Co-Based Electrocatalysts. *J. Phys. Chem. B* **2005**, *109*, 16718−16724.
(50) Fujii, S.; Enoki, T. Nanographene and Graphene Edges: Electronic Structure and Nanofabrication. *Acc. Chem. Res.* **2013**, *46*, 2202−2210.
(51) Murray, A. T.; Surendranath, Y. Reversing the Native Aerobic Oxidation Reactivity of Graphitic Carbon: Heterogeneous Metal-Free Alkene Hydrogenation. *ACS Catal.* **2017**, *7*, 3307−3312.

https://dx.doi.org/10.1021/acs.chemmater.0c02664
Chem. Mater. 2020, 32, 8512−8521